



## RESEARCH ARTICLE

10.1029/2022JD036790

### Key Points:

- Punjab, India experienced cascading delays in the monsoon rice growing season and postmonsoon crop residue burning from 2003 to 2019
- District-level delays vary from 1 to 4 weeks with a longitudinal east-west gradient, where western districts experienced the largest delays
- Delays in postmonsoon fires have consistently led to increased air quality degradation across north India from 2008 to 2019

### Supporting Information:

Supporting Information may be found in the online version of this article.

### Correspondence to:

T. Liu,  
tianjialiu@g.harvard.edu

### Citation:

Liu, T., Mickley, L. J., Patel, P. N., Gautam, R., Jain, M., Singh, S., et al. (2022). Cascading delays in the monsoon rice growing season and postmonsoon agricultural fires likely exacerbate air pollution in north India. *Journal of Geophysical Research: Atmospheres*, 127, e2022JD036790. <https://doi.org/10.1029/2022JD036790>

Received 16 MAR 2022

Accepted 27 OCT 2022

### Author Contributions:

**Conceptualization:** T. Liu, L. J. Mickley  
**Data curation:** T. Liu, P. N. Patel, R. Gautam, M. Jain, S. Singh  
**Formal analysis:** T. Liu, P. N. Patel, R. Gautam  
**Funding acquisition:** T. Liu  
**Investigation:** T. Liu, P. N. Patel, R. Gautam  
**Methodology:** T. Liu, L. J. Mickley, P. N. Patel, R. Gautam, M. Jain, S. Singh  
**Supervision:** L. J. Mickley  
**Validation:** T. Liu

© 2022 The Authors.

This is an open access article under the terms of the [Creative Commons Attribution-NonCommercial License](https://creativecommons.org/licenses/by-nc/4.0/), which permits use, distribution and reproduction in any medium, provided the original work is properly cited and is not used for commercial purposes.

# Cascading Delays in the Monsoon Rice Growing Season and Postmonsoon Agricultural Fires Likely Exacerbate Air Pollution in North India

T. Liu<sup>1</sup>, L. J. Mickley<sup>2</sup>, P. N. Patel<sup>3,4</sup>, R. Gautam<sup>5</sup>, M. Jain<sup>6</sup>, S. Singh<sup>6</sup>, Balwinder-Singh<sup>7</sup>, R. S. DeFries<sup>8</sup>, and M. E. Marlier<sup>9</sup>

<sup>1</sup>Department of Earth and Planetary Sciences, Harvard University, Cambridge, MA, USA, <sup>2</sup>John A. Paulson School of Engineering and Applied Sciences, Harvard University, Cambridge, MA, USA, <sup>3</sup>Jet Propulsion Laboratory, California Institute of Technology, Pasadena, CA, USA, <sup>4</sup>Oak Ridge Associated Universities, Oak Ridge, TN, USA, <sup>5</sup>Environmental Defense Fund, Washington, DC, USA, <sup>6</sup>School for Environment and Sustainability, University of Michigan, Ann Arbor, MI, USA, <sup>7</sup>International Maize and Wheat Improvement Center (CIMMYT)-India Office, New Delhi, India, <sup>8</sup>Department of Ecology, Evolution, and Environmental Biology, Columbia University, New York, NY, USA, <sup>9</sup>Department of Environmental Health Sciences, University of California, Los Angeles, Los Angeles, CA, USA

**Abstract** Over the past two decades, smoke aerosols from crop residue burning have increasingly degraded postmonsoon (October–November) air quality in north India. We use satellite data and atmospheric modeling to investigate whether cascading delays in monsoon rice growth and postmonsoon fires over 2003–2019 have exacerbated the already poor urban air quality downwind of the fires. Beginning in 2008, a government effort to combat groundwater depletion in Punjab mandated rice sowing until closer to the arrival of monsoon rains. We find evidence of district-level delays in the timing of both monsoon rice growth and postmonsoon fires, which vary from 1 to 4 weeks with largely an east-west gradient. These delays are correlated spatially ( $r = 0.51–0.77$ ), with northern and western districts in Punjab, which rely less on groundwater for irrigation, tending to have the greatest delays. Had the delays in fire activity not occurred, we estimate that cities downwind and near the fire source would have consistently seen less smoke-related fine particulate matter ( $PM_{2.5}$ ), on average ranging from 11% to 21% for New Delhi, Bathinda, and Jind during 2008–2019. This net benefit of earlier postmonsoon burning could have been even larger given that (a) a longer rice-to-wheat transition could incentivize farmers to find alternatives to burning crop residues; and (b) background  $PM_{2.5}$  is less abundant earlier in the season, decreasing the likelihood of extreme pollution episodes. Strategies aiming to mitigate air pollution while conserving groundwater may be more effective by promoting an earlier monsoon growing season in districts with less groundwater depletion.

**Plain Language Summary** During the postmonsoon period from October to November, farmers in northwest India have increasingly burned rice residues to quickly clear fields and prepare to plant winter wheat. As seen by satellites, these agricultural fires emit large amounts of smoke that travel to nearby rural areas and populous urban centers, such as New Delhi, contributing to severe air pollution episodes. Beginning in 2008, a government effort to combat groundwater depletion in the state of Punjab mandated rice planting until closer to the arrival of monsoon rains. However, delays in rice planting have led to delays in the timing of postmonsoon agricultural burning. Our modeling results show consistently lower air quality in nearby cities as delayed fires coincide with meteorological conditions that are more favorable for trapping smoke near the surface. Delays in the fire season also shorten the transition period from rice to wheat, thus increasing fire activity further. Strategies aiming to mitigate air pollution in north India may be more effective by stemming the delays in the postmonsoon fire season.

## 1. Introduction

In India, the northwestern states of Punjab and Haryana, the so-called “breadbasket,” are a major rice and wheat-producing region. Many farmers burn crop residues to quickly and cheaply clear fields when transitioning between the monsoon and winter crops in a primarily rice-wheat rotation (Liu et al., 2020; Vadrevu et al., 2011). Agricultural intensification, mechanization, and labor shortages helped sustain and spread the practice of postharvest crop residue burning in spite of government bans (Jethva et al., 2019; Liu et al., 2019; Shyamsundar et al., 2019).

**Visualization:** T. Liu

**Writing – original draft:** T. Liu

**Writing – review & editing:** T. Liu, L. J. Mickley, P. N. Patel, R. Gautam, M. Jain, S. Singh, Balwinder-Singh, R. S. DeFries, M. E. Marlier

Most of the agriculture is dependent on groundwater-based irrigation, and overconsumption has led to unsustainable decline in the water table decline at a rate of  $-2 \text{ cm yr}^{-1}$  in north India from 2002 to 2013 (Asoka et al., 2017). In response, the Punjab and Haryana governments enacted legislation in 2008–2009 to delay monsoon rice sowing (i.e., sow paddy nursery and transplant paddy) closer to the monsoon onset (Rodell et al., 2018; Singh, 2009) to conserve groundwater by minimizing the need for irrigation. (Hereafter, we refer to the date of transplanting rice paddy, which takes place a few weeks after sowing paddy nursery, as the “rice sowing date.”) Moreover, the earliest paddy sowing date, mandated as 10 June in Punjab in 2008, has not remained static, shifting to 15 June 2014, 20 June 2018, and finally to 13 June 2019 (The Indian Express, 2019). Delays in rice sowing shorten the postmonsoon turnaround between monsoon rice harvests and winter wheat sowing, further elevating fire as an attractive option for rice residue management (Balwinder-Singh et al., 2019; Jethva et al., 2019; Liu et al., 2021). Previous observational and modeling studies show that postmonsoon fires from October to November degrade regional air quality downwind and can exacerbate urban air pollution to hazardous levels (Cusworth et al., 2018; Jethva et al., 2018; Kaskaoutis et al., 2014; Liu et al., 2018; Ojha et al., 2020; Patel et al., 2021). A key question is whether the  $\sim 2$ -week delay in postmonsoon fires from 2003 to 2018 may have worsened air pollution, regardless of any trends in anthropogenic emissions levels (Liu et al., 2021). Peak fire activity shifts from late October to early November, when meteorological conditions (i.e., cooler temperatures, weak winds) are more conducive to trapping haze within the shallow boundary layer (Gautam et al., 2021; Liu et al., 2018, 2021; Ojha et al., 2020; Sembhi et al., 2020).

Here we use satellite observations and atmospheric modeling to directly link shifts in the monsoon growing season and postmonsoon fire season to increases in air pollution. Previous studies have thus far established a coincident delay in the timing of peak monsoon greenness and postmonsoon fire activity in northwest India at the region or state level (Balwinder-Singh et al., 2019; Jethva et al., 2019; Liu et al., 2019, 2021). If these trends are associated with one another, we should see evidence that: (a) the temporal shifts of peak monsoon greenness are positively correlated with those of postmonsoon fires at the district level; and (b) the timing of the monsoon growing season and postmonsoon fires is positively correlated with the policy-mandated planting dates post-2008. Liu et al. (2021) found that the magnitude of the delay in the postmonsoon fire activity from 2003 to 2016 across Punjab exhibited a longitudinal gradient, with greater delays in western districts ( $>1.5 \text{ days yr}^{-1}$ ) and smaller delays in eastern districts ( $<1 \text{ day yr}^{-1}$ ), and we thus expect a similar pattern in the timing of peak monsoon greenness, as well as other breakpoints in the monsoon growing season (e.g., green-up, senescence). The observed trends in satellite-derived aerosol loading are consistent with both the delay and increased magnitude in postmonsoon fires (Jethva et al., 2019; Liu et al., 2021), which suggests negative air quality impacts downwind due to these cascading delays, as Kant et al. (2022) found. We thus expect further air quality degradation if fires occur even later, but better air quality with no delays in the fire season. Kant et al. (2022), however, did not isolate the effects of the fire season delays from increases in fire activity. Sembhi et al. (2020) found that enhancements in air pollution due to the observed delay in postmonsoon fires from 2016 to 2018 are in fact minimal in cities across the IGP but highly sensitive to year-to-year meteorological variability. Sembhi et al. (2020) designed three scenarios to evaluate air quality impacts from temporal shifts in the postmonsoon fires in their modeling approach, in which the input fire emissions were (a) kept as is (baseline), (b) shifted 10 days earlier, and (c) shifted 10 days later.

In this study, our goals are twofold: (a) to understand the drivers of the delays in the postmonsoon fire season and (b) to quantify the related air quality impacts. First, we present satellite-based evidence that links the delays in rice growing season and postmonsoon fires at the district level in Punjab. We then investigate the connections between these cascading delays and changes in groundwater levels and policy. Second, we use a receptor-oriented Lagrangian plume model to simulate the effect of these delays on downwind air quality at six cities. More specifically, we undertake a more systematic modeling approach than that utilized by Sembhi et al. (2020) by applying fire emissions, artificially shifted 0–21 days forward and backward in time, to the receptor sensitivities generated under a large set of meteorological conditions (2007–2019). By testing the model with many different combinations of fire season start times and meteorological conditions, we can distinguish the effects of timing versus meteorology on the response of air quality downwind.

## 2. Data and Methods

### 2.1. Satellite Fire and Surface Reflectance Data Sets: Temporal Shifts in Fire Activity and Vegetation Greenness

The Moderate Resolution Imaging Spectroradiometer (MODIS) aboard the Terra and Aqua satellites provide two decades of daily observations of fires and surface reflectance. As a measure of fire intensity, we use maxi-

imum Fire Radiative Power (FRP) from the MODIS/Terra and Aqua gridded active fire data sets, MOD14A1 and MYD14A1, at 1-km spatial resolution (Giglio et al., 2016). The Collection 6 MODIS active fire detection algorithm uses a series of contextual tests to identify active fire pixels, or pixels with enhanced thermal infrared signatures relative to the background at the time of the satellite overpass.

As indicators of crop phenology, we derive the Normalized Difference Vegetation Index (NDVI) and Normalized Burn Ratio (NBR) from the 500-m MODIS/Terra MOD09GA surface reflectance at the red (0.65  $\mu\text{m}$ ), near-infrared (0.86  $\mu\text{m}$ ), and shortwave infrared (2.13  $\mu\text{m}$ ) wavelengths (Vermeote et al., 2015). Time series of MODIS-derived vegetation indices have been used extensively to track crop phenology and quantify crop yields in India and globally (Jain et al., 2013; Liu et al., 2021; Lobell et al., 2013; Sakamoto et al., 2005). NDVI and NBR are analogous indices, but NBR's dependence on the shortwave infrared rather than red band make it less susceptible to noise during the summer monsoon, when cloud cover is high (Liu et al., 2021).

Following Liu et al. (2021), we calculate the timing of (a) the breakpoints (start, midpoint, end) in the progression of the postmonsoon fire season and (b) maximum greenness during the monsoon growing season for each district in Punjab from 2003 to 2019. First, we estimate the midpoint of the fire season as the weighted average of the sequence of Julian days, with each day's FRP as the weight. We also use the cumulative FRP time series, normalized by the total seasonal FRP, to derive the timing of the start, midpoint, and end of the fire season, or the day by which 10% ( $\beta = 0.1$ ), 50% ( $\beta = 0.5$ ), and 90% ( $\beta = 0.9$ ) of burning has occurred, respectively, marked here by breakpoints  $\beta$  in the time series. Second, we use cubic splines to smooth the yearly time series of NBR or NDVI. We make an initial guess of the day of maximum monsoon greenness as the second of two local maxima of the year; these two maxima represent the timing of winter wheat and monsoon rice maturity. We define a 300-day window around this initial guess to perform the final spline smoothing. We use the 500-m MODIS global land cover product, MCD12Q1, with the University of Maryland (UMD) scheme to retain only agricultural pixels for analysis (Sulla-Menashe et al., 2019). For NBR and NDVI, we further mask out areas with zero active fire observations from 2003 to 2019 during the postmonsoon period (here defined as September to November).

We then define the “temporal shift” as the linear trend in the timing of breakpoints in the postmonsoon fire season and monsoon growing season from 2003 to 2019. We assess the spatial correlation between the temporal shifts in the postmonsoon burning season and monsoon greenness for districts in Punjab. Our analysis includes 19 districts, where we observe at least one temporal shift that is statistically significant at  $p < 0.05$ . To further examine spatial patterns in monsoon crop phenology, we use the MCD12Q2 annual land cover dynamics product (500 m), which relies on the Enhanced Vegetation Index (EVI) to estimate the key dates in crop cycles, such as green-up, peak, maturity, and senescence (Gray et al., 2019).

The spatial scale of our analysis is limited by the calculation of key fire season progression breakpoints, which requires many observations of active fires. Because each pixel generally burns only once per season in the context of short-lived agricultural fires, it is difficult to infer the timing of the fire season breakpoints on a per-pixel basis. In calculating temporal shifts, aggregating the analysis to a broader spatial scale helps to reduce noise caused by missed fire detections and low-quality observations.

### 2.1.1. Groundwater Levels

Finally, we evaluate how the temporal shifts in the monsoon growing season and postmonsoon burning relate to groundwater levels and irrigation practices. First, we obtained well data from the India Water Resources Information System (India-WRIS, <https://indiawris.gov.in/wris/>, last accessed: 1 January 2021). To match the spatial scale of our crop phenology and fire temporal shift analyses, we use the average district-level groundwater levels in Punjab from 2003 to 2019. Over 300 wells are monitored in Punjab as of 2019. Second, to estimate the district-level percentage of area irrigated by groundwater relative to canal, we use India census data from the Directorate of Economics and Statistics, Department of Agriculture and Cooperation, Ministry of Agriculture (Dacnet: <https://aps.dac.gov.in/LUS/Index.htm>).

### 2.2. STILT Modeling

We use the Stochastic Time-Inverted Lagrangian Transport (STILT) model (<https://uataq.github.io/stilt/>) to quantify the air quality impacts due to temporal shifts in the postmonsoon fire season (Fasoli et al., 2018). STILT uses meteorology-driven particle dispersion to generate influence footprints, which can then be convolved with

**Table 1**  
*Locations of Receptors/Cities Used in STILT Simulations*

Receptor/city	State/province	Country	Coordinates (longitude, latitude)	Population <sup>a</sup> (in millions)
New Delhi	Delhi	India	77.1°E, 28.7°N	16 (urban), 11 (megacity)
Kanpur	Uttar Pradesh	India	80.33°E, 26.45°N	2.9
Lahore	Punjab	Pakistan	74.36°E, 31.52°N	11
Ludhiana	Punjab	India	75.86°E, 30.9°N	1.6
Bathinda	Punjab	India	74.95°E, 30.21°N	0.3
Jind	Haryana	India	76.3°E, 29.33°N	0.2

<sup>a</sup>The populations of Indian cities are from India's 2011 census, while that of Lahore, Pakistan is from Pakistan's 2017 census.

surface emissions to calculate the concentration of chemical species at a given receptor. STILT is based on NOAA's Hybrid Single-Particle Lagrangian Integrated Trajectory (HYSPPLIT) model, which uses meteorological fields to track the trajectories of theoretical particles either backward or forward in time (Stein et al., 2015). STILT takes one step further and uses Gaussian weighting to calculate the “sensitivity” of emissions in each grid cell to the receptor at each time step based on an ensemble of many particles' trajectories, each slightly different due to the stochastic fluctuations applied to simulate turbulent motions in the atmosphere (Fasoli et al., 2018). STILT sensitivity quantifies how much the regional surface flux in a particular grid cell influences the air arriving at a given receptor; its explicit calculation is described in Lin et al. (2003) and Fasoli et al. (2018). Compared to forward models like WRF-Chem or GEOS-Chem, STILT provides a computationally efficient approach to test the influence of multiple emissions scenarios (Cusworth et al., 2018), which in this case differ by timing of peak burning.

We drive STILT, version 2, with daily meteorology from the Global Data Assimilation System (GDAS) at  $0.5^\circ \times 0.5^\circ$  spatial resolution from 2007 to 2018 and the Global Forecast System (GFS) at  $0.25^\circ \times 0.25^\circ$  spatial resolution in 2019. Following Cusworth et al. (2018) and Liu et al. (2020), for each model run, we send 500 air particles backward in time for 120 hr (5 days), starting from a height of 5 m above ground at the receptor. For our region and time of interest, 500 is a reasonable number of particles for our STILT simulations, since the prevailing meteorology (i.e., slow winds, stable boundary layer, and flat terrain) leads to relatively low variation in the trajectories of different particles. The model domain is defined as  $60\text{--}90^\circ\text{E}$  and  $20\text{--}40^\circ\text{N}$ . We follow the methodology in Cusworth et al. (2018), who started each STILT model simulation at 12 p.m. local time to represent the daily smoke  $\text{PM}_{2.5}$  from agricultural fires. Here we calculate the hourly  $\text{PM}_{2.5}$  every 3 hr from 0 to 21 hr local time from October 1 to November 30 of each year to better account for the diurnal variability in station  $\text{PM}_{2.5}$  observations.

We generate STILT footprints for six receptor cities across the IGP: New Delhi, Kanpur, Lahore, Ludhiana, Bathinda, and Jind (Table 1). These six receptors vary in terms of their population, as well as location and proximity relative to the fire source, and are likely representative of pollution impacts in surrounding areas. To obtain the smoke  $\text{PM}_{2.5}$  exposure at the receptor, we multiply the sensitivity footprints with fire emissions rates and integrate across all hourly timesteps. For agricultural fire emissions, we use the SAGE-IGP regional inventory (Liu et al., 2020). SAGE-IGP relies on both satellite observations and household survey data to adjust MODIS FRP for small fires detected by VIIRS, cloud/haze gaps in observations, partial-field burns, and the diurnal cycle of fire activity. When validated against ground-based observations of  $\text{PM}_{2.5}$  in New Delhi and aerosol loading in Kanpur, STILT simulations with SAGE-IGP perform better than those with global fire emissions inventories.

The  $\text{PM}_{2.5}$  exposure at the receptor is calculated as the sum of the emissions rate multiplied by the STILT sensitivity in each  $0.25^\circ \times 0.25^\circ$  grid cells:

$$C = \sum_{t=1}^m \sum_{i=1}^n E_{i,t} S_{i,t}$$

where  $C$  is the  $\text{PM}_{2.5}$  concentration (ppm) at the receptor.  $E$  is the  $\text{PM}_{2.5}$  emission rate ( $\mu\text{mol m}^{-2} \text{s}^{-1}$ ) calculated as the sum of the organic carbon (OC) and black carbon (BC) emission rates ( $2.1\text{OC} + \text{BC}$ ; Cusworth et al., 2018; Koplitz et al., 2018; Turpin & Lim, 2001),  $S$  is the STILT sensitivity ( $\text{ppm}/(\mu\text{mol m}^{-2} \text{s}^{-1})$ ) at  $i$  grid cell and  $t$

hours before the start of the simulation,  $m$  is the total number of hours in the STILT simulation, and  $n$  is the total number of grid cells in the study domain. The  $\text{PM}_{2.5}$  concentration is then converted into units of  $\mu\text{g m}^{-3}$  by using the ideal gas law, with the surface temperature and pressure at the receptor at the start of the STILT simulation.

### 2.2.1. Designing Hypothetical Scenarios to Model the Impact of Temporal Shifts in Fire Activity on Downwind Smoke Exposure

Peak burning during the 2008–2019 fire seasons on average takes place  $\sim 1$ –2 weeks later than during 2003–2007. To estimate the impact of the delayed postmonsoon fire season on downwind smoke exposure, we artificially shift the temporal distribution of each fire season from 2008 to 2019 by magnitudes ranging from 21 days earlier to 21 days later in 1-day intervals, keeping the total emissions level constant. For this more intensive calculation, we use the footprint sensitivities only for 12 p.m. local time, following Cusworth et al. (2018). Based on a sensitivity test for New Delhi, our results using 12 p.m. as the start time of the STILT simulations are likely conservative in terms of the impact on  $\text{PM}_{2.5}$  but as we will see, consistent with results starting at other hours of the day. By calculating STILT footprints using meteorological conditions from 2007 to 2019, we can gauge the sensitivity of  $\text{PM}_{2.5}$  at the receptor to a range of possible meteorological conditions. For each iteration and combination of the temporally shifted fire season and associated meteorology, we estimate the maximum  $\text{PM}_{2.5}$  from a 21-day rolling mean from 15 September to 15 December. In total, we test 43 iterations for each year from 2008 to 2019, and then apply 13 years of meteorology from 2007 to 2019, for 559 iterations total for each year's fire emissions at each receptor. We calculate the 21-day rolling mean as our metric to capture the  $\text{PM}_{2.5}$  relevant to postmonsoon fire activity, 80% of which occur within an approximate 3-week period (Liu et al., 2021). Specifically, we focus on the impact to smoke  $\text{PM}_{2.5}$  if the fire seasons had not been delayed such that peak burning hypothetically matched either (a) the average date from 2003 to 2007 or (b) the earliest peak date among 2003–2007. For each year, we fit a Gaussian curve to the daily FRP time series to determine the peak burning date of the postmonsoon burning season (Liu et al., 2020, 2021).

## 3. Results and Discussion

### 3.1. Delays in Monsoon Rice Growth Led to Delays in Postmonsoon Fires

Across Punjab, we observe a longitudinal gradient in the temporal shifts in both the peak monsoon greenness and midpoint of the postmonsoon burning season, two central metrics discussed in Liu et al. (2021) (Figures 1a and 1b). Western districts experienced more than twofold greater temporal shifts than eastern districts. The spatial correlation of  $r = 0.71$  ( $p < 0.05$ ) in the district-level shifts of the two metrics suggest that delays in the monsoon growing season may drive those in the postmonsoon burning season (Figure 1c). In sensitivity tests, we find that this correlation is consistent ( $r = 0.51$ – $0.77$ ,  $p < 0.05$ ) across various breakpoints during the postmonsoon fire season (start, midpoint, and end) and monsoon growing season (green-up, peak, maturity, senescence, and dormancy), derived from multiple greenness indices (NBR, NDVI, and EVI) (Table 2). Here we focus on Punjab, but we also find temporal shifts in some districts in Haryana and northern Rajasthan, though the linkage between the delays is less clear in those districts. This may arise from greater spatial intra-district heterogeneity in cropping patterns and use of fire for clearing crop residues.

Further, the average day of peak monsoon greenness from 2003 to 2007 is negatively correlated with the temporal shifts in postmonsoon fires ( $r = -0.5$ ,  $p < 0.05$ ) and monsoon greenness ( $r = -0.88$ ,  $p < 0.05$ ), which indicates that those districts that initially sowed rice the earliest also experienced the greatest cascading delays from paddy sowing to postmonsoon burning within the 2003–2019 period (Figure 1d and Figure S1 in Supporting Information S1). The net effect is the closer alignment of the timing of the midpoint of the postmonsoon fire season across districts in later years, as shown by the 53% ( $p < 0.05$ ) overall decrease in the standard deviation of the spatial distribution of the midpoint (Figure S2 in Supporting Information S1). Thus, a higher biomass load is burned within a shorter time window.

One proposed driver of these delays is Punjab's implementation of the Preservation of Subsoil Water Act, 2009, a policy that sets the earliest date by which farmers can sow paddy, which changed from 10 June 2008 to 15 June 2014, 20 June 2018, and 13 June 2019 (The Indian Express, 2019). From 2008 onward, we find a strong correlation ( $p < 0.05$ ) between changes in the policy-mandated paddy sowing date and satellite-derived timing of the monsoon growing season ( $r = 0.77$ ) and postmonsoon fires ( $r = 0.81$ ) (Figure 2). This correlation suggests that farmers generally adhered to the groundwater policy. While the sample size is small, we see that the anomaly

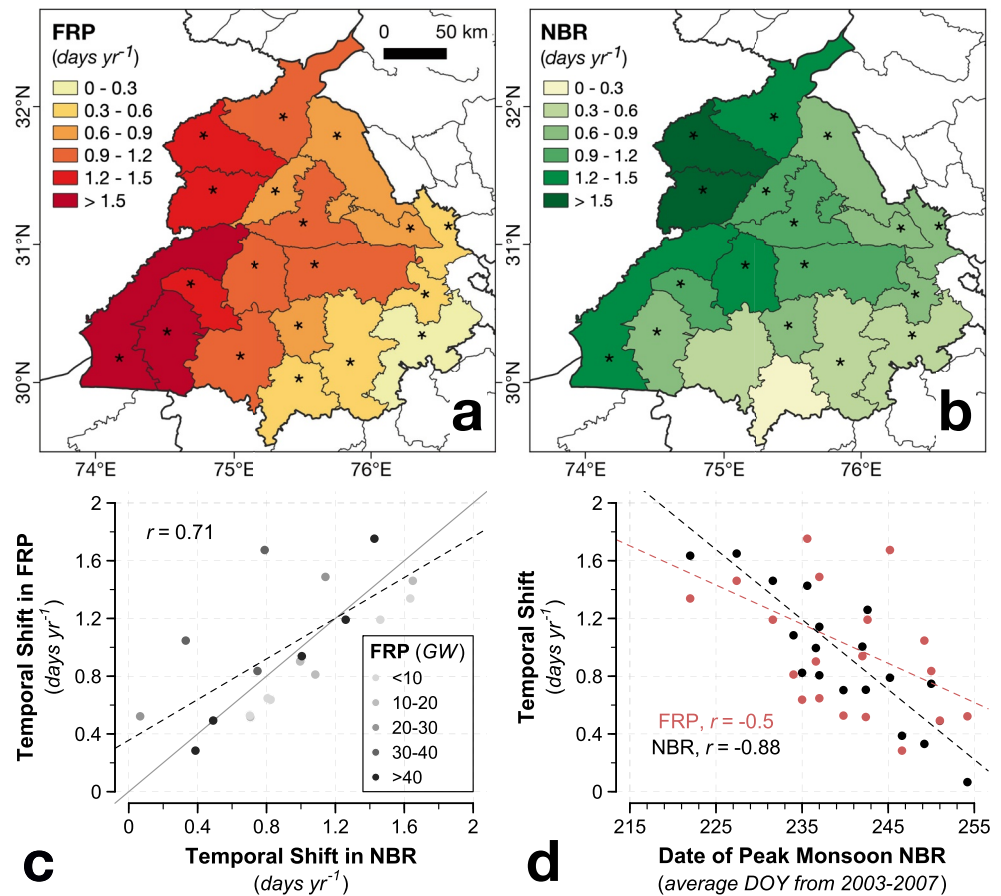


**Figure 1.** Correlation of temporal shifts in postmonsoon fires and peak monsoon greenness by district in Punjab across 2003–2019. We use Fire Radiative Power (FRP) to calculate the midpoint of the postmonsoon fire season and maximum monsoon greenness, indicated by the proxy Normalized Burn Ratio (NBR), to represent the timing of rice maturity. Maps of the district-level temporal shift in (a) FRP and (b) NBR are presented for 19 districts in Punjab. Stars indicate that temporal shift (days yr<sup>-1</sup>) in FRP or NBR is statistically significant ( $p < 0.05$ ) for that district. Districts without statistically significant temporal shifts in both FRP and NBR are omitted from this analysis. (c) Spatial correlation of the temporal shifts in FRP and NBR in districts shown in (a) and (b). The color of the dots denotes the mean postmonsoon FRP. The solid gray line depicts the 1:1 line. (d) Correlation of the average day of year at peak monsoon NBR from 2003 to 2007 and the temporal shifts in NBR and FRP. The correlation coefficients, weighted by the agricultural area of each district, are shown inset.

in the late 2018 growing season and subsequent fires, followed by the 2019 return to the median are consistent with changes in the mandated paddy sowing dates.

In addition to the spatial heterogeneity in the temporal shifts in the monsoon growing season and postmonsoon fires, we also find spatial variation in groundwater usage and trends (Figure 3). For simplicity, we divide Punjab into three regional clusters (north, southwest, and southeast) to illustrate these spatial differences. Observations show that districts in southeast—relative to those districts in the north and southwest—initially sowed paddy the latest (Figure 3a) and experienced the smallest temporal shifts (Figure 3b) but counterintuitively had the highest groundwater usage (Figure 3c) and most severe groundwater depletion after the policy implementation (Figure 3d). These observations appear to show that the groundwater policy was effective—that is, northern districts that needed to drastically shift rice sowing dates to align with that mandated by the policy, indicated by large temporal shifts, subsequently experienced the least severe groundwater depletion. However, one caveat is that southeastern districts were least affected by the policy, indicated by small temporal shifts, continued to suffer from severe groundwater depletion. The groundwater policy broadly slowed falling groundwater levels but can be more effective by setting different target paddy sowing dates across subregions or districts within the state.

**Table 2**

*Correlations Between the Temporal Shifts in the Timing of the Monsoon Growing Season and Postmonsoon Fire Season*

		Postmonsoon fire season (FRP)			
		Midpoint (weighted mean)	Midpoint ( $\beta = 0.5$ )	Start ( $\beta = 0.1$ )	End ( $\beta = 0.9$ )
Monsoon rice growing season		<i>MOD09GA</i>			
	Peak (NBR)	0.71	0.74	0.66	0.63
	Peak (NDVI)	0.72	0.74	0.66	0.65
		<i>MCD12Q2 (EVI)</i>			
	Green-up	0.73	0.75	0.57	0.71
	Maturity	0.67	0.71	0.58	0.64
	Peak	0.65	0.7	0.58	0.61
	Senescence	0.73	0.77	0.68	0.67
	Dormancy	0.56	0.61	0.51	0.52

*Note.* The correlation coefficient  $r$  is calculated for the 19 Punjab districts with statistically significant ( $p < 0.05$ ) temporal shifts in the midpoint of the fire season (using the weighted mean method) and/or peak monsoon greenness (NBR), such as shown in Figures 1 and 2. All correlations are statistically significant at  $p < 0.05$ .

Further observational data, such as survey data with large sample sizes, are needed to robustly link the groundwater policy and its intended effect at the district level to changes in irrigation water management practices. Confounding factors include variation in the type of rice grown (i.e., basmati versus coarse grain), soil texture, and recent shifts in the crops planted (e.g., cotton to rice). Additionally, while changes in precipitation or temperature may explain some interannual variability in the timing of crop phenology or the fire season, the large delay of  $\sim 1$  week observed around the 2008–2009 implementation of the groundwater policy is not reflected in meteorology (Liu et al., 2021). Changes in the earliest rice sowing dates set by the groundwater policy are highly correlated with the timing of crop phenology ( $r = 0.77$ ) and the fire season ( $r = 0.81$ ), which further supports the link between the policy and its cascading effects (Figure 2).

### 3.2. Sensitivity of Downwind Smoke Exposure to Timing of Postmonsoon Fires

We first focus on the effects of temporal shifts of burning on downwind smoke exposure in New Delhi, the most populous megacity in India. As STILT footprints show, air quality in New Delhi is sensitive to fires in Punjab and Haryana due to prevailing northwesterly winds that are consistent year after year (Figure S5 in Supporting Information S1). Figure 4 shows an example of the ratio of modeled smoke  $PM_{2.5}$  in Delhi for the 2017 postmonsoon fire season that is hypothetically shifted forward and backward in time relative to the observed fire season in daily increments. Generally, smoke  $PM_{2.5}$  decreases as the fire season shifts earlier and increases as the fire season shifts later.

If the 2008–2019 postmonsoon burning seasons had not been delayed and occurred earlier by 1–2 weeks on par with the average timing of peak fires observed in 2003–2007, the maximum 21-day mean  $PM_{2.5}$  in New Delhi would on average be reduced by 12% (min:  $-50\%$ , max:  $+32\%$ ) (Figure 5). This result is consistent across various start hours of the day for the STILT simulations, with our choice of 12 p.m. likely leading to conservative estimates (Figure S6 in Supporting Information S1). The range of this response to the temporal shift in burning indicates that year-to-year meteorology drives substantial variability in downwind  $PM_{2.5}$ . Nonetheless, in nine of the 12 years from 2008 to 2019, Delhi would have experienced lower  $PM_{2.5}$  in the absence of the shift toward later peak burning (Figure 5). Next, we apply a range of meteorology-driven footprint sensitivities (2007–2019) to each year's fire emissions. We find that the median  $PM_{2.5}$  would be reduced by 17% (11%–22%), compared with the business-as-usual scenario of delayed burning. If we further shift fire emissions by another 4 days earlier such that peak burning matches that of the earliest peak date from 2003 to 2007, the decrease in median  $PM_{2.5}$  would be  $\sim 1.5$  times as high at 26% (20%–37%). Conversely, if the postmonsoon fire season continues to shift later, we find that the  $PM_{2.5}$  burden in downwind areas will likely increase further under our 13-year range of meteorological conditions.

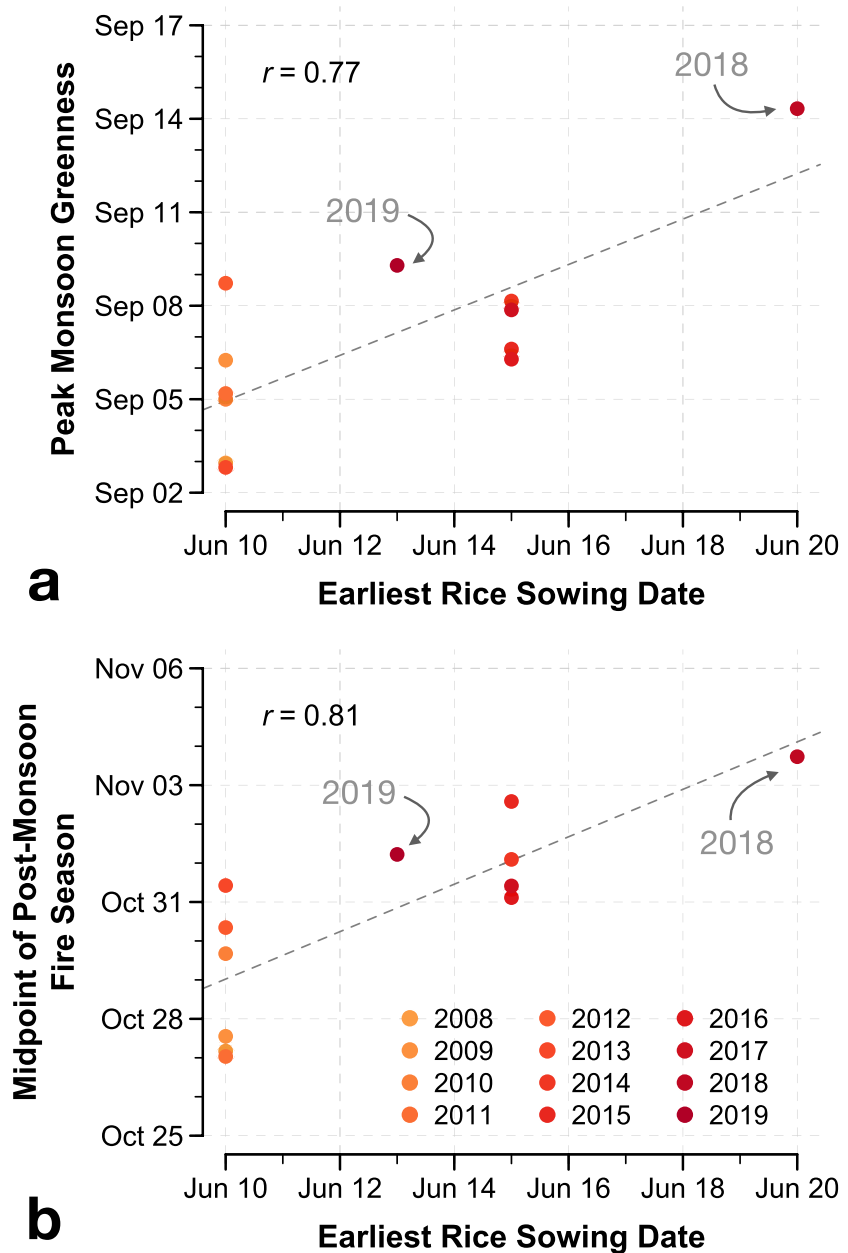


**Figure 2.** Correlation between the earliest rice sowing dates and timing of the peak monsoon greenness and midpoint of the postmonsoon fire season in Punjab from 2008 to 2019. The earliest rice paddy sowing dates mandated by the Punjab Preservation of Subsoil Water Act are shown with respect to the satellite-derived (a) peak monsoon greenness and (b) midpoint of the postmonsoon fire season. Dates for the peak monsoon greenness and midpoint of the postmonsoon fire season are averaged across the districts in Punjab shown in Figure 1, weighted by the districts' agricultural area. The color of the dots corresponds to the year. The correlation coefficients are shown inset and are statistically significant at  $p < 0.05$ .

Figure 6 illustrates why delays in the postmonsoon fire season—without any consideration of increases in fire activity—can lead to increased  $PM_{2.5}$  in New Delhi. Afternoon mixing layer heights in New Delhi decrease from  $\sim 1,900$  m in October to  $\sim 1,200$  m by mid-November, pointing to weak ventilation conditions that favor aerosol buildup near the surface (Figure 6a). Simultaneously, the spatial average of STILT sensitivity for New Delhi, weighted by fire emissions, steadily rises during this period, suggesting that air quality in New Delhi is increasingly susceptible to degradation from regional fires with time (Figure 6b). Due to the delays in the fire season, peak fires occur when New Delhi is  $\sim 41\%$  more sensitive to regional fires in 2008–2019 than in 2003–2007. As the postmonsoon transitions to winter, weak winds, cooler temperatures, and a shallow boundary



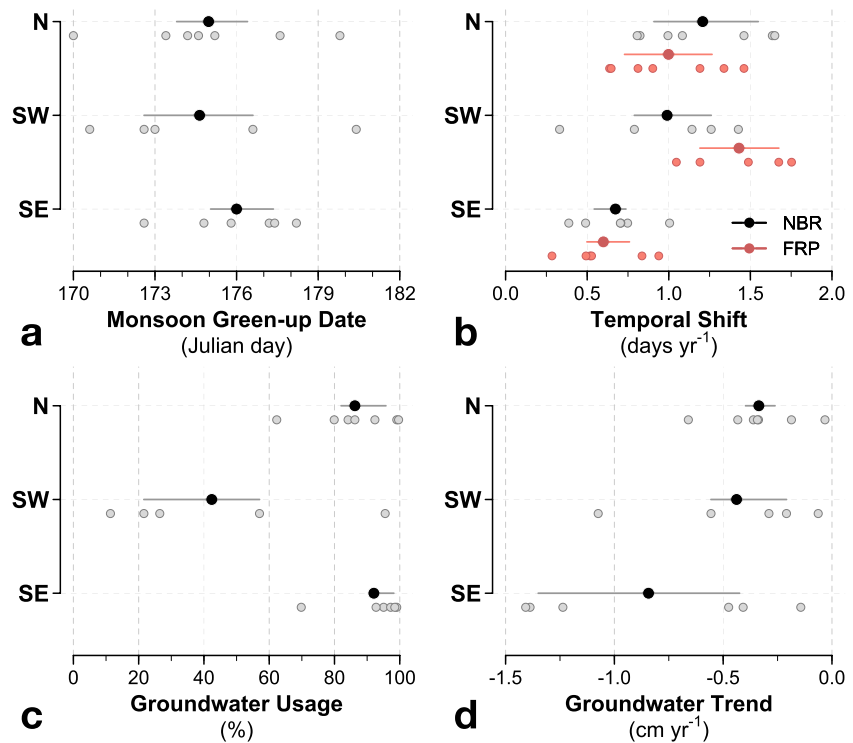


**Figure 3.** Regional summary of district-level trends in phenology, fires, and groundwater levels in Punjab, India. (a) Monsoon green-up date from 2003 to 2007, (b) temporal shifts in the timing of the peak monsoon greenness (i.e., maximum Normalized Burn Ratio (NBR)) and midpoint of the postmonsoon fire season (i.e., weighted average using Fire Radiative Power (FRP)) from 2003 to 2019, denoted by black and red, respectively, (c) groundwater usage as a percentage of total area irrigated by wells and canals, and (d) groundwater level trends from 2008 to 2019. Here Punjab is split into three regions: north (N), southwest (SW), and southeast (SE). Solid dots represent the trend or value averaged across districts in that region, and lines represent the 25th to 75th percentile range. Light gray dots represent the trend or value for individual districts.

layer may also drive a steady increase in background  $PM_{2.5}$ , which would further reduce air quality (Section S2.2 and Figure S7 in Supporting Information S1). Further analysis is needed to dissect how different meteorological parameters (i.e., winds, boundary layer dynamics, diurnal variability, and temperature inversion) contribute to air quality degradation.

Next, we examine how air quality responds to delays in fire activity in five other cities across the IGP: Kanpur, Lahore, Ludhiana, Bathinda, and Jind (Table 2 and Figure 7). These six cities represent a diverse sample of receptors that range in proximity and direction relative to the fire-dominant regions. This is evident in the range in 21-day average smoke  $PM_{2.5}$  of 15–173  $\mu g m^{-3}$  experienced at each receptor (Figure 8 and Table S2 in Supporting Information S1). Figure 9 shows the spatial pattern of each city's mean STILT sensitivity, weighted by the daily smoke  $PM_{2.5}$  at the receptor. We find that if postmonsoon fires had not been delayed during 2008–2019, receptors that are downwind and close to the fire source (i.e., Bathinda, Jind, and New Delhi)—and with the highest 21-day average smoke  $PM_{2.5}$ —consistently see decreases in smoke  $PM_{2.5}$  of 11%–21% on average (Figure 9 and Table S2 in Supporting Information S1). In contrast, the effect of the fire season delays on smoke  $PM_{2.5}$  is highly variable from year to year in Kanpur, Lahore, and Ludhiana, where smoke  $PM_{2.5}$  is more sensitive to changes in meteorology. Specifically, Lahore and Ludhiana are often upwind of the fires due to prevailing northwesterly winds (Liu et al., 2018; Patel et al., 2021), while Kanpur is the farthest receptor from the fire source.

Our modeling design has some limitations. For our hypothetical simulations of smoke  $PM_{2.5}$  where fire emissions are shifted backward in time, we assume that fire emissions shift uniformly across all grid cells. In reality, as seen in our satellite-based analysis, western districts in northwest India experienced greater delays in postmonsoon fire activity than eastern districts (Figure 1a). While our atmospheric modeling approach simplifies this heterogeneity of the observed delays, the consistent decreases in smoke  $PM_{2.5}$  as fire emissions gradually shift earlier in 1-day intervals—and increases in smoke  $PM_{2.5}$  with further delays—lend confidence to our results (Figure 4). The

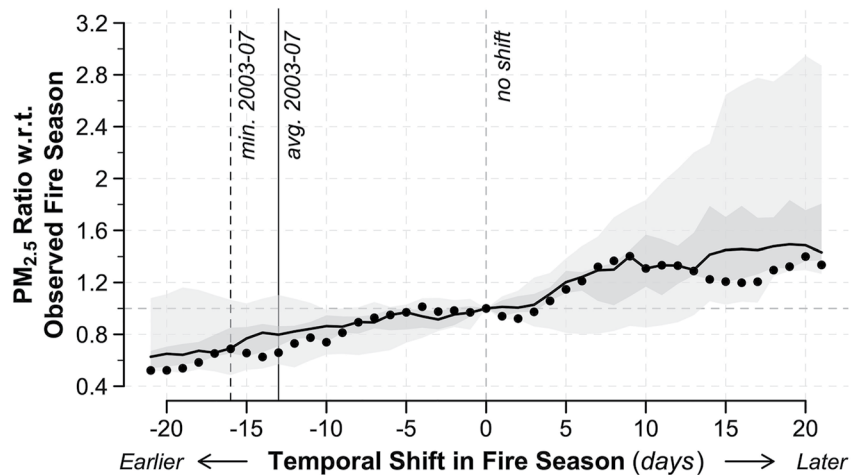


**Figure 4.** Effect of temporal shifts in the postmonsoon agricultural fire season on downwind  $PM_{2.5}$  in New Delhi in 2017. The response of seasonal maximum  $PM_{2.5}$  concentrations is shown for hypothetical shifts in the fire season from 21 days earlier to 21 days later, for 2017 fire emissions and a range of meteorological scenarios. For each scenario, we calculate the maximum smoke  $PM_{2.5}$  in New Delhi from a 21-day rolling mean from 1 October to 30 November for a hypothetical shift in the fire season relative to the one observed. The median ratio derived from varying STILT footprint sensitivities by meteorology from 2007 to 2019 is shown as the solid curve. The dark gray envelope shows the 25th–75th percentiles in ratios, and the light gray envelope shows the 5th–95th percentiles. Dots indicate the relative smoke  $PM_{2.5}$  using only 2017 meteorology. The vertical black lines show the change in  $PM_{2.5}$  if the 2017 postmonsoon fire season is shifted earlier to two baselines: (1) average from 2003 to 2007 (solid) and (2) earliest peak date among 2003–2007 (dashed).

magnitude of fire emissions is also not well-constrained, as satellites may miss fires with low thermal anomalies and those that occur outside the overpass times and during periods with thick haze and smog (Liu et al., 2020). However, this study focuses on relative changes in  $PM_{2.5}$ , for which the magnitude of fire emissions is less

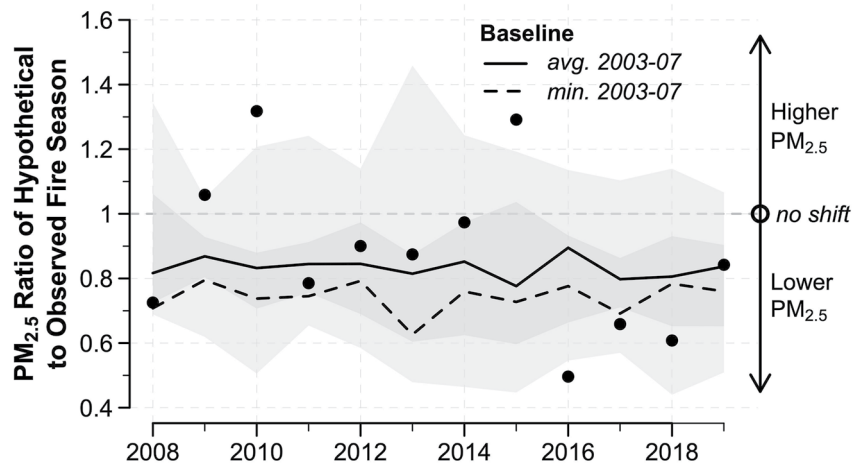


**Figure 5.** Effect on  $PM_{2.5}$  in New Delhi from 2008 to 2018 if the postmonsoon agricultural fire season had not experienced delays relative to the 2003–2007 period. The response of seasonal  $PM_{2.5}$  concentrations is shown for two different hypothetical shifts in the fire season for a range of meteorological scenarios. For each year, that season's fire emissions are shifted earlier by the number of days between the peak burning day of each fire season and that of two baselines: (1) average from 2003 to 2007 (solid line) and (2) earliest during 2003–2007 (dashed line). Smoke  $PM_{2.5}$  in New Delhi is calculated as the maximum of 21-day rolling means from 1 October to 30 November for a hypothetical fire season that is shifted earlier relative to one that was observed. The medians derived from varying STILT footprint sensitivities from 2007 to 2019 are shown as the solid and dashed lines. Dots indicate the smoke  $PM_{2.5}$  estimated with the meteorology and fire emissions of the given year relative to that for a hypothetical fire season aligned with the 2003–2007 average peak timing. Shaded envelopes denote the 25th–75th percentile range in relative smoke  $PM_{2.5}$  (dark gray) and the 5th–95th percentile range (light gray), again using fire emissions of the given year and the 2003–2007 peak timing, but meteorology in all available years from 2008 to 2019.

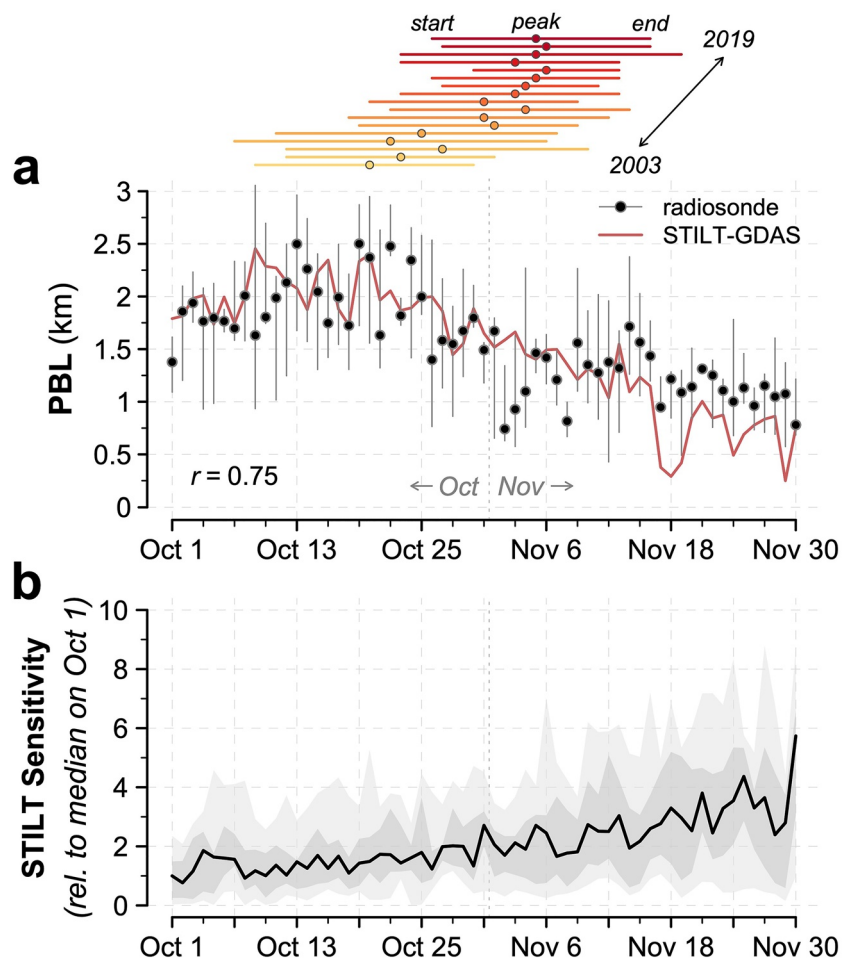


**Figure 6.** Compression of daily afternoon boundary layer heights and increase in average Stochastic Time-Inverted Lagrangian Transport (STILT) sensitivities for New Delhi during the postmonsoon burning season. (a) The median PBL heights from radiosonde data (black dots) and from STILT with Global Data Assimilation System (GDAS) meteorology (red line) at 5:30 p.m. local time from 2003 to 2019. The October–November decrease in PBL heights is also observed during other afternoon hours from GDAS meteorology (not shown). Gray segments depict the 25th–75th percentiles of the radiosonde data, and the correlation coefficient between radiosonde and STILT-GDAS PBL is shown inset. Segments at the top show the timing of the start, peak, and end of the postmonsoon burning season in Punjab and Haryana from 2003 to 2019, with warmer colors indicating later years. (b) Daily average STILT sensitivity footprints for New Delhi are weighted by the average 2003–2019 postmonsoon SAGE-IGP dry matter emissions. The STILT sensitivities are shown as normalized values relative to the mean STILT sensitivity on 1 October. The black line indicates normalized median STILT sensitivity across 2007–2019, while the dark gray envelope denotes the 25th–75th percentiles, and the light gray envelope shows the 5th–95th percentiles.

important. Finally, while we show that there are associations between the groundwater policy, delays in monsoon season sowing date, and delays in burning at the end of the monsoon season, it is possible that other factors, such as changes in crop type or variety, may explain some of these associations. Future work should examine the causal relationship between these variables using large-scale survey data and/or causal inference methods.

### 3.3. Contextualizing the Importance of Delays in the Postmonsoon Fire Season

Sembhi et al. (2020) suggest that the impact of the delay in the postmonsoon fire season on regional air quality may be small relative to that of the increase in fire activity or meteorological variability. Under a larger range of meteorological conditions, our results generally show a consistent decrease in smoke  $PM_{2.5}$  had the fire season been earlier; the  $PM_{2.5}$  decreases are robust in Jind, Bathinda, and New Delhi, three downwind receptors that experience high 21-day mean smoke  $PM_{2.5}$  of 44–173  $\mu g m^{-3}$ . Additionally, two contextual factors may enhance

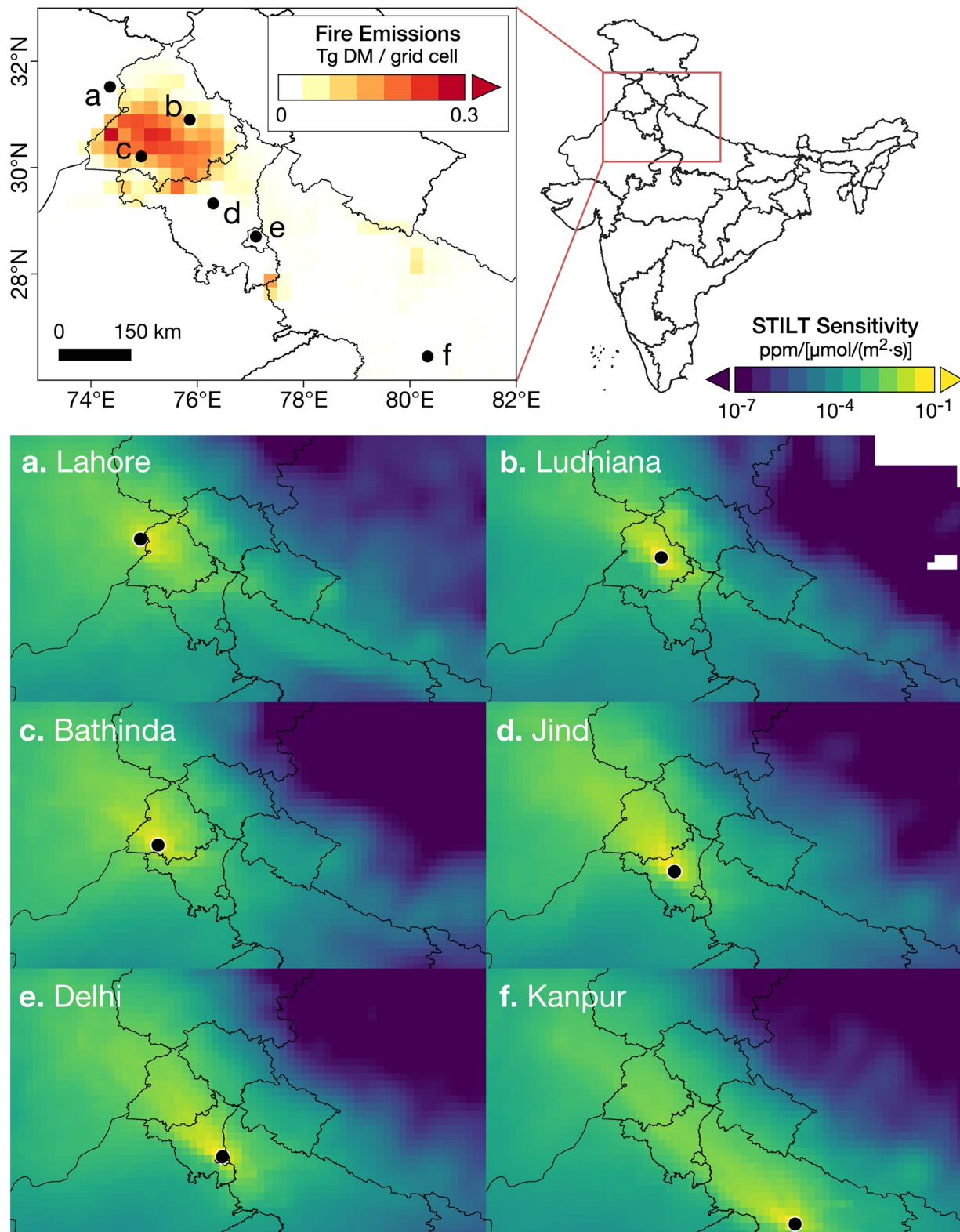


**Figure 7.** STILT sensitivity footprints for six receptors. (Top panel) Location of the six selected STILT receptors, overlaid on SAGE-IGP postmonsoon dry matter burned, averaged across 2008–2019: (a) Lahore, (b) Ludhiana, (c) Bathinda, (d) Jind, (e) New Delhi, and (f) Kanpur. (Bottom panels) STILT sensitivities are averaged first from 1 October to 30 November of each year, weighted by the smoke  $\text{PM}_{2.5}$  at the receptor, and then across 2008–2019. Note that the color bar increments for the STILT sensitivities are logarithmic. The  $\text{PM}_{2.5}$  at each receptor is calculated as the sum of the STILT sensitivity multiplied by the fire emissions across all grid cells and time steps of the model simulation.

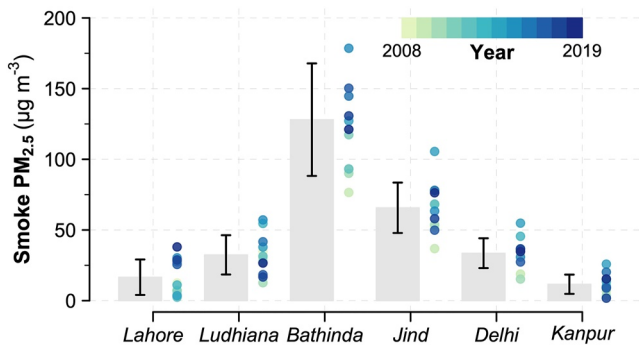


**Figure 8.**  $PM_{2.5}$  concentrations in six cities during the postmonsoon agricultural fire season from 2008 to 2019. Maximum smoke  $PM_{2.5}$  from a 21-day rolling mean from 1 October to 30 November. Bars depict the average from 2008 to 2019, and segments denote  $\pm 1\sigma$ . Dots denote the maximum 21-day rolling mean  $PM_{2.5}$  in each year, with lighter colors representing earlier years and darker colors, later years. Here the years of the fire emissions and meteorology match, and no additional meteorological conditions are considered.

the importance of the delay to regional air pollution mitigation strategies: (a) the linkage between the increase and delay in fire activity and (b) the superposition of high smoke  $PM_{2.5}$  on increased background  $PM_{2.5}$  with potential aerosol-radiation feedbacks. Gautam et al. (2021) and Pan et al. (2015) previously underscored the role of secondary aerosol formation in the context of heavy aerosol pollution in northern India. We describe these factors in greater detail below.

First, the increase and delay in fires are intrinsically linked—that is, the cascading delays in the rice growing season and postmonsoon burning compress the harvest-to-sowing window, driving further use of fire as farmers attempt to efficiently clear their fields of crop residues (Liu et al., 2020). Consequently, fire activity is particularly intense later in the fire season in early to mid-November (Liu et al., 2021), when thick haze and smog can obscure fires from satellite detection and lead to underestimates in fire emissions (Cusworth et al., 2018; Liu et al., 2020). Several factors—including the delay in the fire season, increasing use of combine harvesters, and increasing crop production—likely all drive the overall increase in fire activity (Jethva et al., 2019; Liu et al., 2021). It is difficult to disentangle the influence of each factor, as farmers often cite multiple, interconnected reasons for burning rice residues, including saving time and cost, overcoming the short

harvest-to-sowing transition window, labor shortages, and lacking technology and incentives to manage the residues (Bhuvaneshwari et al., 2019; Liu et al., 2020).

Second, background  $PM_{2.5}$  from primarily anthropogenic pollution sources increases from postmonsoon to winter, at least in part because of meteorological conditions favoring pollution buildup. For example, we find that the background  $PM_{2.5}$  steadily increased by 1.06–1.66  $\mu g m^{-3}$  per day in New Delhi from October to December, though this apparent increase may not be captured by standard atmospheric modeling frameworks (Figures S7, S8 and Section S2.2 in Supporting Information S1). Superposing smoke  $PM_{2.5}$  on higher background  $PM_{2.5}$  later in the burning season increases the risk of extremely polluted days ( $>250 \mu g m^{-3}$ ), when wide-reaching emergency measures are taken to protect public health and safety, such as by canceling flights, halting construction, and closing schools (The Guardian, 2017; The Times of India, 2017). As experienced in early-to-mid-November

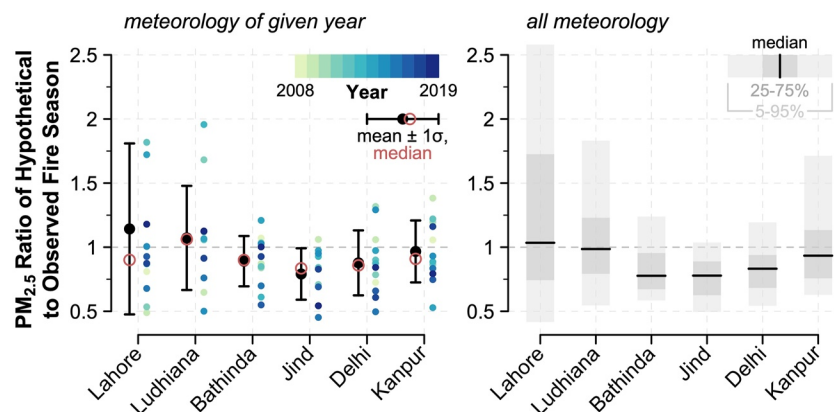


**Figure 9.** Effect on  $PM_{2.5}$  in six cities from 2008 to 2019 if the postmonsoon agricultural fire season had not experienced delays relative to the 2003–2007 period. Fire emissions are shifted earlier by the number of days between the peak burning day of each fire season and that of the 2003–2007 average. (Left panel) Maximum smoke  $PM_{2.5}$  from a 21-day rolling mean from 1 October to 30 November for a hypothetical fire season that is shifted earlier relative to one that was observed. For each city, the  $PM_{2.5}$  ratio is shown as the median across all years (red circles), mean  $\pm 1\sigma$  (black dots and bars), and for individual years (colored dots). Cities are arranged from east to west along the  $x$  axis. (Right panel) Same as left panel, except the fire emissions of each year are applied to STILT sensitivities for all years from 2007 to 2019 to show the impact of a range of possible meteorological conditions. The  $PM_{2.5}$  ratio is averaged across meteorological years by quantiles. The horizontal bars show the median; the dark gray envelopes show the 25th–75th percentile range, and the light gray envelopes show the 5th–95th percentile range.

in 2017, the buildup of smoke aerosols in northwest India can lead to both large spikes in  $PM_{2.5}$  concentrations and regional smog that persists into the early afternoon, a phenomenon typically observed in winter (Gautam et al., 2007, 2021; Ghude et al., 2017; Liu et al., 2021). Due to the heterogeneity in the postmonsoon fire season delay across districts, the timing of burning across all districts is now more closely aligned, increasing regional smoke concentrations on peak burning days. Thus, models such as that in Sembhi et al. (2020) may not have captured the full impact of the delayed fire season on downwind  $PM_{2.5}$ . In addition, the positive feedback of aerosol-radiation interactions, by strengthening temperature inversions and increasing boundary layer stability, may have further enhanced  $PM_{2.5}$  concentrations, as has been previously examined over China (Gao et al., 2015; Miao et al., 2019; Qiu et al., 2017; Wang, He et al., 2018; Wang, Peng, et al., 2018). For north India, Gautam et al. (2021) used satellite, ground-based, and reanalysis data to show that a decadal trend in aerosol-induced warming potentially strengthened lower tropospheric stability and increased smog-heavy, low visibility days. Due to computational cost, many atmospheric modeling studies do not account for two-way aerosol interactions with meteorology (Li et al., 2017; Petäjä et al., 2016). Secondary aerosol formation, an important driver of severe haze episodes (Li et al., 2017)—particularly from fires (Palm et al., 2020)—is also not well-constrained in models and in modeled representations of smoke loading which has been previously underscored in multi-model analyses focusing on north India (Pan et al., 2015).

#### 4. Conclusion

In summary, we present evidence that delays in the monsoon rice growing season are strongly associated with similar delays in the postmonsoon burning season, resulting in a cascading effect that further degrades downwind air quality. Along with weak northwesterly winds during the postmonsoon, this is driven by the lower boundary layer and cooler surface air temperatures typically observed in November. We find that in the absence of the delay in biomass burning during 2008–2019, cities that are both downwind and near the fire source—New Delhi, Bathinda, and Jind—would have consistently seen 11%–21% less smoke  $PM_{2.5}$  than occurred if the same fires happened earlier in the season. Some of the range of uncertainty arises from the influence of plausible meteorological conditions, that is, variability in wind patterns and boundary layer heights that influence the sensitivity of the receptor to smoke; for example, in New Delhi, we find that  $PM_{2.5}$  would have on average been reduced by 12% from 2008 to 2019, but the year-to-year range varies from –50% to +32%. However, despite variable meteorology, nine of the 12 years examined would have experienced lower  $PM_{2.5}$  with had there been no delays in burning. While we show that the delays alone have led to increased  $PM_{2.5}$  in downwind areas, the later fire season also drives further fire activity, thus compounding the net negative impact on  $PM_{2.5}$  exposure. Our work identifies those districts in Punjab where delays in postmonsoon burning have occurred with relatively less groundwater depletion. This suggests that a revised groundwater policy allowing earlier sowing dates in such districts could improve air quality in north India while conserving groundwater.

#### Data Availability Statement

MODIS land cover and active fire data sets are publicly available through the Google Earth Engine public data catalog and distributed by NASA's Earthdata platform. The specific data sets used in this study are: MOD14A1 active fires (<https://doi.org/10.5067/MODIS/MOD14A1.006>), MYD14A1 active fires (<https://doi.org/10.5067/MODIS/MYD14A1.006>), MOD09GA surface reflectance (<https://doi.org/10.5067/MODIS/MOD09GA.006>), MCD12Q1 land cover (<https://doi.org/10.5067/MODIS/MCD12Q1.006>), and MCD12Q2 land cover dynamics (<https://doi.org/10.5067/MODIS/MCD12Q2.006>).

#### Acknowledgments

This work was supported by a National Science Foundation Graduate Research Fellowship awarded to T. Liu (DGE1745303). STILT model simulations in this paper were run on the FASRC Cannon cluster supported by the FAS Division of Science Research Computing Group at Harvard University. We thank John Lin, Derek Mallia, and Meghna Agarwala for their helpful comments.

#### References

- Asoka, A., Gleeson, T., Wada, Y., & Mishra, V. (2017). Relative contribution of monsoon precipitation and pumping to changes in groundwater storage in India. *Nature Geoscience*, 10(2), 109–117. <https://doi.org/10.1038/ngeo2869>
- Balwinder-Singh, McDonald, A. J., Srivastava, A. K., & Gerard, B. (2019). Tradeoffs between groundwater conservation and air pollution from agricultural fires in northwest India. *Nature Sustainability*, 2, 580–583. <https://doi.org/10.1038/s41893-019-0304-4>
- Bhuvaneshwari, S., Hettiarachchi, H., & Meegoda, J. N. (2019). Crop residue burning in India: Policy challenges and potential solutions. *International Journal of Environmental Research and Public Health*, 16(5), 832. <https://doi.org/10.3390/ijerph16050832>
- Cusworth, D. H., Mickley, L. J., Sulprizio, M. P., Liu, T., Marlier, M. E., Defries, R. S., et al. (2018). Quantifying the influence of agricultural fires in northwest India on urban air pollution in Delhi, India. *Environmental Research Letters*, 13(4), 044018. <https://doi.org/10.1088/1748-9326/aab303>

- Fasoli, B., Lin, J. C., Bowling, D. R., Mitchell, L., & Mendoza, D. (2018). Simulating atmospheric tracer concentrations for spatially distributed receptors: Updates to the stochastic time-inverted Lagrangian Transport model's R interface (STILT-R version 2). *Geoscientific Model Development*, 11(7), 2813–2824. <https://doi.org/10.5194/gmd-11-2813-2018>
- Gao, Y., Zhang, M., Liu, Z., Wang, L., Wang, P., Xia, X., et al. (2015). Modeling the feedback between aerosol and meteorological variables in the atmospheric boundary layer during a severe fog-haze event over the North China Plain. *Atmospheric Chemistry and Physics*, 15(8), 4279–4295. <https://doi.org/10.5194/acp-15-4279-2015>
- Gautam, R., Hsu, N. C., Kafatos, M., & Tsay, S. (2007). Influences of winter haze on fog/low cloud over the Indo-Gangetic plains. *Journal of Geophysical Research*, 112, D05207. <https://doi.org/10.1029/2005JD007036>
- Gautam, R., Patel, P. N., Singh, M. K., Liu, T., Mickley, L. J., Jethva, H., & DeFries, R. S. (2021). Extreme smog challenge of northern India intensified by increasing lower tropospheric stability. *npj Climate and Atmospheric Science*. Preprint. <https://doi.org/10.31223/X5X049>
- Ghude, S. D., Bhat, G. S., Prabhakaran, T., Jenamani, R. K., Chate, D. M., Safai, P. D., et al. (2017). Winter fog experiment over the Indo-Gangetic plains of India. *Current Science*, 112(4), 767–784. <https://doi.org/10.18520/cs/v112/i04/767-784>
- Giglio, L., Schroeder, W., & Justice, C. O. (2016). The collection 6 MODIS active fire detection algorithm and fire products. *Remote Sensing of Environment*, 178, 31–41. <https://doi.org/10.1016/j.rse.2016.02.054>
- Gray, J., Sulla-Menashe, D., & Friedl, M. A. (2019). User Guide to Collection 6 MODIS land cover dynamics (MCD12Q2) product. <https://doi.org/10.5067/MODIS/MCD12Q1.006>
- Jain, M., Mondal, P., DeFries, R. S., Small, C., & Galford, G. L. (2013). Mapping cropping intensity of smallholder farms: A comparison of methods using multiple sensors. *Remote Sensing of Environment*, 134, 210–223. <https://doi.org/10.1016/j.rse.2013.02.029>
- Jethva, H., Chand, D., Torres, O., Gupta, P., Lyapustin, A., & Patadia, F. (2018). Agricultural burning and air quality over northern India: A Synergistic analysis using NASA's A-train satellite data and ground Measurements. *Aerosol and Air Quality Research*, 18(7), 1756–1773. <https://doi.org/10.4209/aaqr.2017.12.0583>
- Jethva, H., Torres, O., Field, R. D., Lyapustin, A., Gautam, R., & Kayetha, V. (2019). Connecting crop productivity, residue fires, and air quality over northern India. *Scientific Reports*, 9, 16594. <https://doi.org/10.1038/s41598-019-52799-x>
- Kant, Y., Chauhan, P., Natwariya, A., Kannaujia, S., & Mitra, D. (2022). Long term influence of groundwater preservation policy on stubble burning and air pollution over North-West India. *Scientific Reports*, 12, 2090. <https://doi.org/10.1038/s41598-022-06043-8>
- Kaskaoutis, D. G., Kumar, S., Sharma, D., Singh, R. P., Kharol, S. K., Sharma, M., et al. (2014). Effects of crop residue burning on aerosol properties, plume characteristics, and long-range transport over northern India. *Journal of Geophysical Research: Atmospheres*, 119, 5424–5444. <https://doi.org/10.1002/2013JD021357>
- Kopplitz, S. N., Mickley, L. J., Jacob, D. J., Marlier, M. E., DeFries, R. S., Gaveau, D. L. A., et al. (2018). Role of the Madden-Julian Oscillation in the transport of smoke from Sumatra to the Malay Peninsula during severe Non-El Niño haze Events. *Journal of Geophysical Research: Atmospheres*, 123, 6282–6294. <https://doi.org/10.1029/2018JD028533>
- Li, M., Zhang, Q., Kurokawa, J. I., Woo, J. H., He, K., Lu, Z., et al. (2017). Mix: A mosaic Asian anthropogenic emission inventory under the international collaboration framework of the MICS-Asia and HTAP. *Atmospheric Chemistry and Physics*, 17(2), 935–963. <https://doi.org/10.5194/acp-17-935-2017>
- Li, Z., Guo, J., Ding, A., Liao, H., Liu, J., Sun, Y., et al. (2017). Aerosol and boundary-layer interactions and impact on air quality. *National Science Review*, 4(6), 810–833. <https://doi.org/10.1093/nsr/nwx117>
- Lin, J. C., Gerbig, C., Wofsy, S. C., Andrews, A. E., Daube, B. C., Davis, K. J., & Grainger, C. A. (2003). A near-field tool for simulating the upstream influence of atmospheric observations: The Stochastic Time-Inverted Lagrangian Transport (STILT) model. *Journal of Geophysical Research*, 108(D16), 4493. <https://doi.org/10.1029/2002JD003161>
- Liu, T., Marlier, M. E., DeFries, R. S., Westervelt, D. M., Xia, K. R., Fiore, A. M., et al. (2018). Seasonal impact of regional outdoor biomass burning on air pollution in three Indian cities: Delhi, Bengaluru, and Pune. *Atmospheric Environment*, 172, 83–92. <https://doi.org/10.1016/j.atmosenv.2017.10.024>
- Liu, T., Marlier, M. E., Karambelas, A., Jain, M., Singh, S., Singh, M. K., et al. (2019). Missing emissions from post-monsoon agricultural fires in northwestern India: Regional limitations of MODIS burned area and active fire products. *Environmental Research Communications*, 1, 011007. <https://doi.org/10.1088/2515-7620/ab056c>
- Liu, T., Mickley, L. J., Gautam, R., Singh, M. K., DeFries, R. S., & Marlier, M. E. (2021). Detection of delay in post-monsoon agricultural burning across Punjab, India: Potential drivers and consequences for air quality. *Environmental Research Letters*, 16, 014014. <https://doi.org/10.1088/1748-9326/abcc28>
- Liu, T., Mickley, L. J., Singh, S., Jain, M., DeFries, R. S., & Marlier, M. E. (2020). Crop residue burning practices across north India inferred from household survey data: Bridging gaps in satellite observations. *Atmospheric Environment X*, 8, 100091. <https://doi.org/10.1016/j.aea.2020.100091>
- Lobell, D. B., Ortiz-Monasterio, J. I., Sibley, A. M., & Sohu, V. S. (2013). Satellite detection of earlier wheat sowing in India and implications for yield trends. *Agricultural Systems*, 115, 137–143. <https://doi.org/10.1016/j.agsy.2012.09.003>
- Miao, Y., Li, J., Miao, S., Che, H., Wang, Y., Zhang, X., et al. (2019). Interaction between planetary boundary layer and PM<sub>2.5</sub> pollution in Megacities in China: A review. *Current Pollution Reports*, 5(4), 261–271. <https://doi.org/10.1007/s40726-019-00124-5>
- Ojha, N., Sharma, A., Manish, K., Girach, I., Ansari, T. U., Sharma, S. K., et al. (2020). On the widespread enhancement in fine particulate matter across the Indo-Gangetic Plain towards winter. *Scientific Reports*, 10, 5862. <https://doi.org/10.1038/s41598-020-62710-8>
- Palm, B. B., Peng, Q., Fredrickson, C. D., Lee, B. H., Garofalo, L. A., Pothier, M. A., et al. (2020). Quantification of organic aerosol and Brown carbon evolution in fresh wildfire plumes. *Proceedings of the National Academy of Sciences of the United States of America*, 117(47), 29469–29477. <https://doi.org/10.1073/pnas.2012218117>
- Pan, X., Chin, M., Gautam, R., Bian, H., Kim, D., Colarco, P. R., et al. (2015). A multi-model evaluation of aerosols over South Asia: Common problems and possible causes. *Atmospheric Chemistry and Physics*, 15(10), 5903–5928. <https://doi.org/10.5194/acp-15-5903-2015>
- Patel, K., Bhandari, S., Gani, S., Campmier, M. J., Kumar, P., Habib, G., et al. (2021). Sources and dynamics of submicron aerosol during the Autumn onset of the air pollution season in Delhi, India. *ACS Earth and Space Chemistry*, 5, 118–128. <https://doi.org/10.1021/acsearthspacechem.0c00340>
- Petäjä, T., Järvi, L., Kerminen, V. M., Ding, A. J., Sun, J. N., Nie, W., et al. (2016). Enhanced air pollution via aerosol-boundary layer feedback in China. *Scientific Reports*, 6, 1–6. <https://doi.org/10.1038/srep18998>
- Qiu, Y., Liao, H., Zhang, R., & Hu, J. (2017). Simulated impacts of direct radiative effects of scattering and absorbing aerosols on surface layer aerosol concentrations in China during a heavily polluted event in February 2014. *Journal of Geophysical Research: Atmospheres*, 122, 5955–5975. <https://doi.org/10.1002/2016JD026309>
- Rodell, M., Famiglietti, J. S., Wiese, D. N., Reager, J. T., Beaudoin, H. K., Landerer, F. W., & Lo, M. H. (2018). Emerging trends in global freshwater availability. *Nature*, 557(7707), 651–659. <https://doi.org/10.1038/s41586-018-0123-1>

- Sakamoto, T., Yokozawa, M., Toritani, H., Shibayama, M., Ishitsuka, N., & Ohno, H. (2005). A crop phenology detection method using time-series MODIS data. *Remote Sensing of Environment*, *96*(3–4), 366–374. <https://doi.org/10.1016/j.rse.2005.03.008>
- Sembhi, H., Wooster, M., Zhang, T., Sharma, S., Singh, N., Agarwal, S., et al. (2020). Post-monsoon air quality degradation across Northern India: Assessing the impact of policy-related shifts in timing and amount of crop residue burnt. *Environmental Research Letters*, *15*, 104067. <https://doi.org/10.1088/1748-9326/aba714>
- Shyamsundar, P., Springer, N. P., Tallis, H., Polasky, S., Jat, M. L., Sidhu, H. S., et al. (2019). Fields on fire: Alternatives to crop residue burning in India. *Science*, *365*, 536–538. <https://doi.org/10.1126/science.aaw4085>
- Singh, K. (2009). Act to save groundwater in Punjab: Its impact on water table, electricity subsidy and environment. *Agricultural Economics Research Review*, *22*, 365–386. <https://doi.org/10.1016/j.tej.2009.04.008>
- Stein, A. F., Draxler, R. R., Rolph, G. D., Stunder, B. J. B., Cohen, M. D., & Ngan, F. (2015). NOAA's HYSPLIT atmospheric transport and dispersion modeling System. *Bulletin of the American Meteorological Society*, *96*(12), 2059–2077. <https://doi.org/10.1175/BAMS-D-14-00110.1>
- Sulla-Menashe, D., Gray, J. M., Abercrombie, S. P., & Friedl, M. A. (2019). Hierarchical mapping of annual global land cover 2001 to present: The MODIS Collection 6 Land Cover product. *Remote Sensing of Environment*, *222*, 183–194. <https://doi.org/10.1016/j.rse.2018.12.013>
- The Guardian. (2017). Delhi doctors declare pollution emergency as smog chokes city. Retrieved from <https://www.theguardian.com/world/2017/nov/07/delhi-india-declares-pollution-emergency-as-smog-chokes-city>
- The Indian Express. (2019). How advancing paddy sowing by a week helps Punjab farmers, and Congress. Retrieved from <https://indianexpress.com/article/explained/how-advancing-paddy-sowing-by-a-week-helps-punjab-farmers-and-congress-5725114/>
- The Times of India. (2017). Air pollution: NGT bans construction, waste burning in Delhi. Retrieved from <https://timesofindia.indiatimes.com/city/delhi/air-pollution-ngt-bans-construction-waste-burning-in-delhi/articleshow/61576103.cms>
- Turpin, B. J., & Lim, H. J. (2001). Species contributions to PM<sub>2.5</sub> mass concentrations: Revisiting common assumptions for estimating organic mass. *Aerosol Science and Technology*, *35*, 602–610. <https://doi.org/10.1080/02786820119445>
- Vadrevu, K. P., Ellicott, E., Badarinarath, K. V. S., & Vermote, E. (2011). MODIS derived fire characteristics and aerosol optical depth variations during the agricultural residue burning season, north India. *Environmental Pollution*, *159*(6), 1560–1569. <https://doi.org/10.1016/j.envpol.2011.03.001>
- Vermote, E. F., Roger, J. C., & Ray, J. P. (2015). MODIS surface reflectance User's Guide: Collection 6. Retrieved from <http://modis-sr.ltdri.org>
- Wang, H., Peng, Y., Zhang, X., Liu, H., Zhang, M., Che, H., et al. (2018). Contributions to the explosive growth of PM<sub>2.5</sub> mass due to aerosol-radiation feedback and decrease in turbulent diffusion during a red alert heavy haze in Beijing-Tianjin-Hebei, China. *Atmospheric Chemistry and Physics*, *18*(23), 17717–17733. <https://doi.org/10.5194/acp-18-17717-2018>
- Wang, X., He, X., Miao, S., & Dou, Y. (2018). Numerical simulation of the influence of aerosol radiation effect on urban boundary layer. *Science China Earth Sciences*, *61*(12), 1844–1858. <https://doi.org/10.1007/s11430-018-9260-0>

## References From the Supporting Information

- Bey, I., Jacob, D. J., Yantosca, R. M., Logan, J. A., Field, B. D., Fiore, A. M., et al. (2001). Global modeling of tropospheric chemistry with assimilated meteorology: Model description and evaluation. *Journal of Geophysical Research*, *106*(D19), 23073–23095. <https://doi.org/10.1029/2001JD000807>
- Dhillon, B. S., & Kumar, R. (2021). Short-duration paddy varieties can turn the tide. *The Tribune India*. Retrieved from <https://www.tribuneindia.com/news/punjab/short-duration-paddy-varieties-can-turn-the-tide-264670>
- Mahajan, G., Bharaj, T. S., & Timsina, J. (2009). Yield and water productivity of rice as affected by time of transplanting in Punjab, India. *Agricultural Water Management*, *96*(3), 525–532. <https://doi.org/10.1016/j.agwat.2008.09.027>
- The Tribune India. (2019). Crumbling canal system takes toll on groundwater. Retrieved from <https://www.tribuneindia.com/news/archive/punjab/crumbling-canal-system-takes-toll-on-groundwater-790245>
- Wang, Y. X., McElroy, M. B., Jacob, D. J., & Yantosca, R. M. (2004). A nested grid formulation for chemical transport over Asia: Applications to CO. *Journal of Geophysical Research*, *109*, D22307. <https://doi.org/10.1029/2004JD005237>